THE JOURNAL OF PHYSICAL CHEMISTRY B

Article

pubs.acs.org/JPCB

Toward Temperature-Dependent Coarse-Grained Potentials of Side-Chain Interactions for Protein Folding Simulations. II. Molecular Dynamics Study of Pairs of Different Types of Interactions in Water at Various Temperatures

Emil Sobolewski,[†] Stanisław Ołdziej,[†,§] Marta Wiśniewska,[‡] Adam Liwo,[‡,§] and Mariusz Makowski*[,‡,§]

[†]Laboratory of Biopolymer Structure, Intercollegiate Faculty of Biotechnology, University of Gdańsk, Medical University of Gdańsk, Kładki 24, 80-822 Gdańsk, Poland

[‡]Faculty of Chemistry, University of Gdańsk, ul. Sobieskiego 18, 80-952 Gdańsk, Poland

[§]Baker Laboratory of Chemistry and Chemical Biology, Cornell University, Ithaca, New York 14853-1301, United States

Supporting Information

ABSTRACT: By means of molecular dynamics simulations of 15 pairs of molecules selected to model the interactions of nonpolar, nonpolar and polar, nonpolar and charged, polar, and polar and charged side chains in water, we determined the potentials of mean force (PMFs) of pairs of interacting molecules in water as functions of distance between the interacting particles or their distance and orientations at three temperatures: 283, 323, and 373 K, respectively. The systems were found to fall into the following four categories as far as the temperature dependence of the PMF is concerned: (i) pairs for which association is entropy-driven, (ii) pairs for which association is energy-driven, (iii) pairs of positively charged solute molecules, for which association is energy-driven with unfavorable entropy change, and (iv) the remaining systems for which temperature dependence is weak. For each pair of PMFs, entropic and energetic contributions have been discussed.

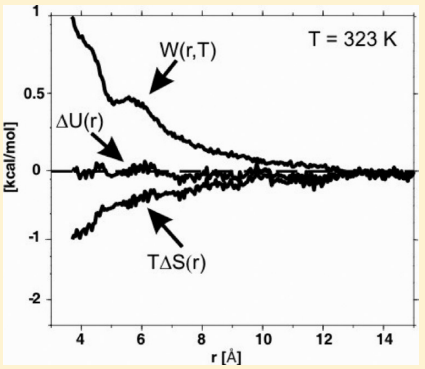

INTRODUCTION

Most of the coarse-grained force-fields currently used for protein-structure prediction and simulations of protein dynamics and thermodynamics do not have any temperature dependence, which is inconsistent with their physical origin as potentials of mean force (PMFs).[1−4] Temperature dependence has recently been introduced[5] in the UNRES force-field developed in our laboratory, in the multibody-interaction terms that originate from higher-order terms in the cluster-cumulant expansion of the backbone-interaction PMF of polypeptide chains.[6] On the other hand, effective water-mediated interactions between side chains in proteins, in particular the hydrophobic interactions, which are related to free energy of cavity formation and the entropy of solvent reorganization, depend on temperature. For example,[7] Némethy and Scheraga found that hydrophobic aggregation at constant pressure is known to be more pronounced as temperature increases. Water-mediated interactions between side chains in proteins are one of the principal factors that contribute to protein stability,[8] and, consequently, their understanding and correct treatment in force fields is essential.

It should be noted that we assume that the side-chain-interaction potentials are pairwise additive. This means that we consider only the first-order factors comprising the side chain−side chain interactions related. Clearly, higher-order factors, as well as factors involving local and peptide-group interactions along with side chain−side chain interactions should also be considered. However, the pairwise-additive model of effective side chain-side chain interactions seems to work well with the UNRES model.[4−6]

Several simulation studies carried out at constant volume[9] (NVT) and at constant pressure[10−12] (NPT) confirmed that the depth of the contact minimum increases with temperature, while the effect of temperature on the height of the desolvation barrier and the depth of the solvent-separated minimum is smaller. In these studies, diverse methodologies and water models were used for PMF determination, namely, simulations of 8 solute molecules in a periodic box with TIP3P, TIP4P, TIP5P, SPC, or SPCE water and direct calculation of solute pair-correlation function,[11,12] thermodynamic integration and the SPC water model,[9] and the particle-insertion method and the TIP4P water model.[10] Recently,[13] we carried out molecular dynamics (MD) simulations for a pair of interacting methane particles at different temperatures in NVT or NPT protocols in TIP3P water model.[14] On the basis of our MD results, we

Special Issue: B: Harold A. Scheraga Festschrift

Received: December 30, 2011
Revised: April 3, 2012
Published: April 5, 2012

determined the PMF and dimensionless PMF curves. The aim of that research was to find simple rules that could be implemented in computing the PMF at different temperatures without the necessity of performing expensive simulations. We found that, for methane−methane pairs in water at constant volume, the plots of dimensionless PMF as functions of the distance between nonpolar particles determined for various temperatures overlap very well in the regions of minimum and maximum. This suggests that, in order to obtain expression for the effective interaction energy at constant volume, we just need to scale a dimensionless hydrophobic interaction potential, specific for a given pair of hydrophobic particles, by the RT factor, where R is a universal gas constant and T is temperature.

We also found that, for the dimensionless PMF curves of methane−methane pairs determined at constant pressure, the depth of contact minimum increases with increasing temperature, and the height of the desolvation maximum and the depth of the solvent-separated minimum decrease with temperature. However, no clear quantitative relationship was found between the PMFs or between dimensionless PMFs determined at various temperatures from constant-pressure simulations. The results of our research[13] are in agreement with the literature data.[11]

One important conclusion from the work discussed above[13] is that the assumption that the depth of the minimum of the side chain−side chain interaction component of coarse-grained potentials is independent of temperature neglects its actual increase with increasing temperature. The neglect of this increase is equivalent to assuming that the strength of the simulated interactions between nonpolar side chains decreases with temperature at contact distance, which does not agree with the experimental finding that increasing temperature leads to hydrophobic association, or early protein-folding stages. Consequently, the absence of temperature dependence of the potentials of side-chain interactions can introduce artifacts into the results of simulations and lead to false conclusions.

From the above considerations it follows that any force field that uses an implicit water model, i.e., such that its part representing solvent-mediated interaction has the sense of a PMF, should incorporate the dependence of the solvent-dependent part on temperature to reproduce the thermodynamics of protein folding correctly. In most coarse-grained force fields, including the UNRES force field developed in our laboratory,[4−6] the solvent-related part is included in the effective potentials for side chain−side chain interactions. In our previous paper[13] we initiated the work on introducing temperature dependence in the effective side chain−side chain interaction potential of the UNRES force field. Earlier,[15−20] we performed an extensive work of the replacement of the present statistical side chain−side chain interaction potentials in the UNRES force field with physics-based potentials, as well as some more general studies of water-mediated interactions between nonpolar, charged, or nonpolar and charged solutes in water.[21−24] The present work is the extension of our previous studies to the temperature dependence of the PMFs of models of selected side-chain pairs with different polarity and charge in water. We have selected fifteen pairs of nonpolar (*n*-propane to model hydrophobic side chains), polar (propanamide to model Asn or Gln side chain), and charged (ethylammonium cation, propionate anion, and 1-methylguanidinium cation to model Lys, Asp or Glu, and Arg side chains, respectively). As in our previous work,[13,15−24] we determined the respective PMFs by means of umbrella-sampling MD simulations at constant volume.

METHODS

MD simulations were carried out with the AMBER suite of programs,[25,26] using the AMBER 7.0 force field at temperatures T = 283, 323, and 373 K in the NVT ensemble (constant number of particles, volume, and temperature). The integration step was 2 fs at each temperature. The bond lengths and bond angles of water molecules were maintained constant by means of the SETTLE algorithm.[27] The following 15 pairs of solute molecules were selected as model systems: propanamide−propanamide (to model Asn or Gln−Asn or Gln interactions), *n*-propane−*n*-propane (to model hydrophobic interactions), ethylammonium cation−propionamide (to model Lys−Asn or Gln interactions), *n*-propane−ethylammonium cation (to model hydrophobic particle−Lys interactions), *n*-propane−propionate anion (to model hydrophobic particle−Asp or Glu interactions), *n*-propane−ethylammonium cation (to model hydrophobic particle−Lys interactions), propionate anion−propnionate anion (to model Asp or Glu−Asp or Glu interactions), ethylammonium cation−propionate anion (to model Asp or Glu−Lys interactions), ethylammonium cation−ethylammonium cation (to model Lys−Lys interactions), propanamide−propionate anion (to model Asn or Gln−Asp or Glu interactions), 1-methylguanidinium cation−propanamide (to model Arg−Asn or Gln interactions), 1-methylguanidinium cation−*n*-propane (to model Arg−hydrophobic particle interactions), 1-methylguanidinium cation−1-methylguanidinium cation (to model Arg−Arg interactions), 1-methylguanidinium cation−ethylammonium cation (to model Arg−Lys interactions), and 1-methylguanidinium cation−propionate anion (to model Arg−Asp or Glu interactions); these systems will hereafter be referred to as PrN−PrN, PrP−PrP, EtN−PrN, PrP−PrN, PrP−PrA, PrP−EtN, PrA−PrA, EtN−PrA, EtN−EtN, PrN−PrA, Gua−PrN, Gua−PrP, Gua−Gua, Gua−EtN, and Gua−PrA, respectively. Each of the pairs of molecules was placed in a periodic box containing TIP3P water molecules.[14] The TIP3P model of water is valid in the temperatures studied in this work.[14] Box sizes and the numbers of water molecules in each box are collected in Table S1 of the Supporting Information.

The charges on the atoms of the solute molecules, needed for the AMBER 7.0 force field, were determined for each side-chain model by using a standard procedure,[14] by fitting the point-charge molecular electrostatic potential to the molecular electrostatic potential computed by using the electronic wave function calculated at the restricted Hartree−Fock (RHF) level with the 6-31G* basis set. The program GAMESS[28] was used to carry out the quantum-mechanical calculations, while the program RESP[29] of the AMBER 7.0 package was used to compute the fitted charges. The charges and the AMBER atom types are shown in Figure S1 of the Supporting Information.

Each MD simulation consisted of a 200 ps equilibration period followed by 10 ns production calculations. A 9.0 Å cutoff was imposed on Lennard-Jones interactions, while particle-mesh Ewald summation with a 9.0 Å cutoff was used to compute electrostatic interactions. For each system, a series of 24 windows was run with different harmonic restraint potentials imposed on the distance between the atoms closest to the center of mass of each of the particles, as given by eq 1.

$$V_i(r) = k(r - r_i^0)^2 \quad (1)$$

dx.doi.org/10.1021/jp212593h | J. Phys. Chem. B 2012, 116, 6844−6853

where k is a force constant [k = 2 kcal/(mol × Å^2) was used], r is the interparticle distance, and r_i^0 is the center of the restraint in the ith simulation (window); the values of r^0 were 3.5, 4,4.5, 5.0, 5.5, 6.0, 6.5, 7.0, 7.5, 8.0, 8.5, 9.0, 9.5, 10.0, 10.5, 11.0, 11.5, 12.0, 12.5, 13.0, 13.5, 14.0, 14.5, and 15.0 Å. A total of 50 000 configurations was collected for each window at each temperature. For systems with a net charge different from zero, counterions (Cl^- or Na^+) were added to balance the charge of the solute molecules.

We computed two types of PMF plots, i.e., as a function of only the distance between geometrical centers and as a function of the distance between geometrical centers and orientations of interacting particles. The variables defining distance and orientation of the side chains are shown in Figure 1.

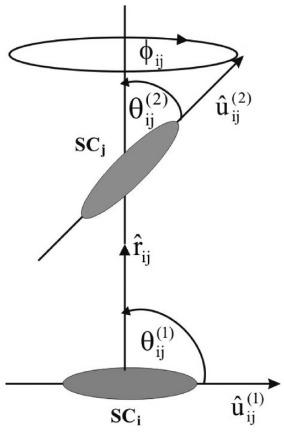

Figure 1. Definition of variables describing the location of two spheroidal particles (i and j) with respect to each other. The vector $\hat{\mathbf{u}}_{ij}^{(1)}$ is the unit vector of the long axis of particle i, $\hat{\mathbf{u}}_{ij}^{(2)}$ is the unit vector of the long axis of particle j, $\hat{\mathbf{r}}_{ij}$ is the unit vector pointing from particle i to particle j, $\theta_{ij}^{(1)}$ and $\theta_{ij}^{(2)}$ are the angles between the vector $\hat{\mathbf{r}}_{ij}$ and vectors $\hat{\mathbf{u}}_{ij}^{(1)}$ and $\hat{\mathbf{u}}_{ij}^{(2)}$, respectively, and ϕ_{ij} is the angle of counterclockwise rotation of the vector $\hat{\mathbf{u}}_{ij}^{(2)}$ about the vector $\hat{\mathbf{r}}_{ij}$ from the plane defined by the vector $\hat{\mathbf{u}}_{ij}^{(1)}$ and vector $\hat{\mathbf{r}}_{ij}$ when looking from the center of particle j toward the center of particle i.

The PMFs were computed from the raw umbrella-sampling simulation data by using the weighted histogram analysis method (WHAM).[30,31] Because we used very large water boxes in our studies, we can safely assume that the PMF is zero at the largest distances encountered in a simulation. In Figure 2 we also show the convergence plot for the most complex system Gua−Gua obtained at 323 K. As seen in Figure 2 there are only slight differences between PMFs for 25% and 100% configurations. The convergence is achieved as the number of configurations increased. The same convergence was observed for the remaining pairs at all temperatures studied.

In the next section we discuss the PMF dependent only on distance, the dimensionless PMF dependent only on distance, the PMF dependent on distance and orientation, and the dimensionless PMF dependent on distance and orientation. These quantities are defined by eqs 2−5, respectively:

$$W(r;\ T) = -RT\ \ln g(r;\ T) \tag{2}$$

$$\tilde{W}(r;\ T) = -\ln g(r;\ T) \tag{3}$$

$$W(r,\ \theta^{(1)},\ \theta^{(2)},\ \varphi;\ T) = -RT\ \ln g(r,\ \theta^{(1)},\ \theta^{(2)},\ \varphi;\ T) \tag{4}$$

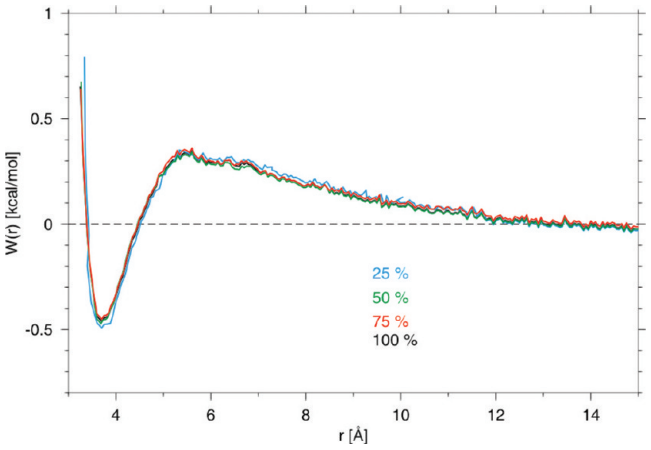

Figure 2. PMF curves for the Gua−Gua dimer for four different numbers of configurations obtained from the umbrella-sampling/WHAM method using the TIP3P water model.[14] The simulations were carried out at a temperature of 323 K. The blue, green, red, and black lines refer to 25% (12 500 configurations), 50% (25 000 configurations), 75% (37 500 configurations), and 100% (50 000 configurations), respectively, of the total number of generated configurations.

$$\tilde{W}(r,\ \theta^{(1)},\ \theta^{(2)},\ \varphi;\ T) = -\ln g(r,\ \theta^{(1)},\ \theta^{(2)},\ \varphi;\ T) \tag{5}$$

where $W(r;T)$ and $\tilde{W}(r;T)$ are the PMF and the dimensionless PMF, respectively, at distance r and absolute temperature T; $g(r;T)$ is the pair correlation function (determined from umbrella-sampling MD simulations followed by postprocessing with WHAM) at distance r and absolute temperature T; $W(r,\theta^{(1)},\theta^{(2)},\phi;T)$ and $\tilde{W}(r,\theta^{(1)},\theta^{(2)},\phi;T)$ are the PMF and the dimensionless PMF, respectively, dependent on distance r and orientation at absolute temperature T; $g(r,\theta^{(1)},\theta^{(2)},\phi;T)$ is the pair correlation function (determined from MD simulations) dependent on distance r and orientation at absolute temperature T, and R is the universal gas constant.

In the Results section, we also show plots of the entropic and energetic contributions to the absolute constant-volume PMF (defined by eq 2). To estimate the entropic and energetic contributions to the PMFs, we numerically differentiated the respective PMFs with respect to temperature by using a symmetrized divided-difference formula with unequal left and right intervals, as given by eq 6. The entropic and energetic contributions were then computed by using eqs 7 and 8, respectively:

$$\frac{\partial W(r,\ T_i)}{\partial T_i} \approx \frac{1}{2}\cdot\left[\frac{W(r,\ T_{i+1}) - W(r,\ T_i)}{T_{i+1} - T_i} + \frac{W(r,\ T_i) - W(r,\ T_{i-1})}{T_i - T_{i-1}}\right] \tag{6}$$

$$\Delta S(r,\ T_i) = -\left(\frac{\partial W(r,\ T_i)}{\partial T_i}\right) \tag{7}$$

$$\Delta U(r,\ T_i) = W(r,\ T_i) + T_i \Delta S(r,\ T_i) \tag{8}$$

where T_{i-1} = 283 K, T_i = 323 K, and T_{i+1} = 373 K. In a later part of our paper, we show results of entropy and energy contributions to the PMFs computed at 323 K, which is in the middle of temperature range studied.

dx.doi.org/10.1021/jp212593h | J. Phys. Chem. B 2012, 116, 6844−6853

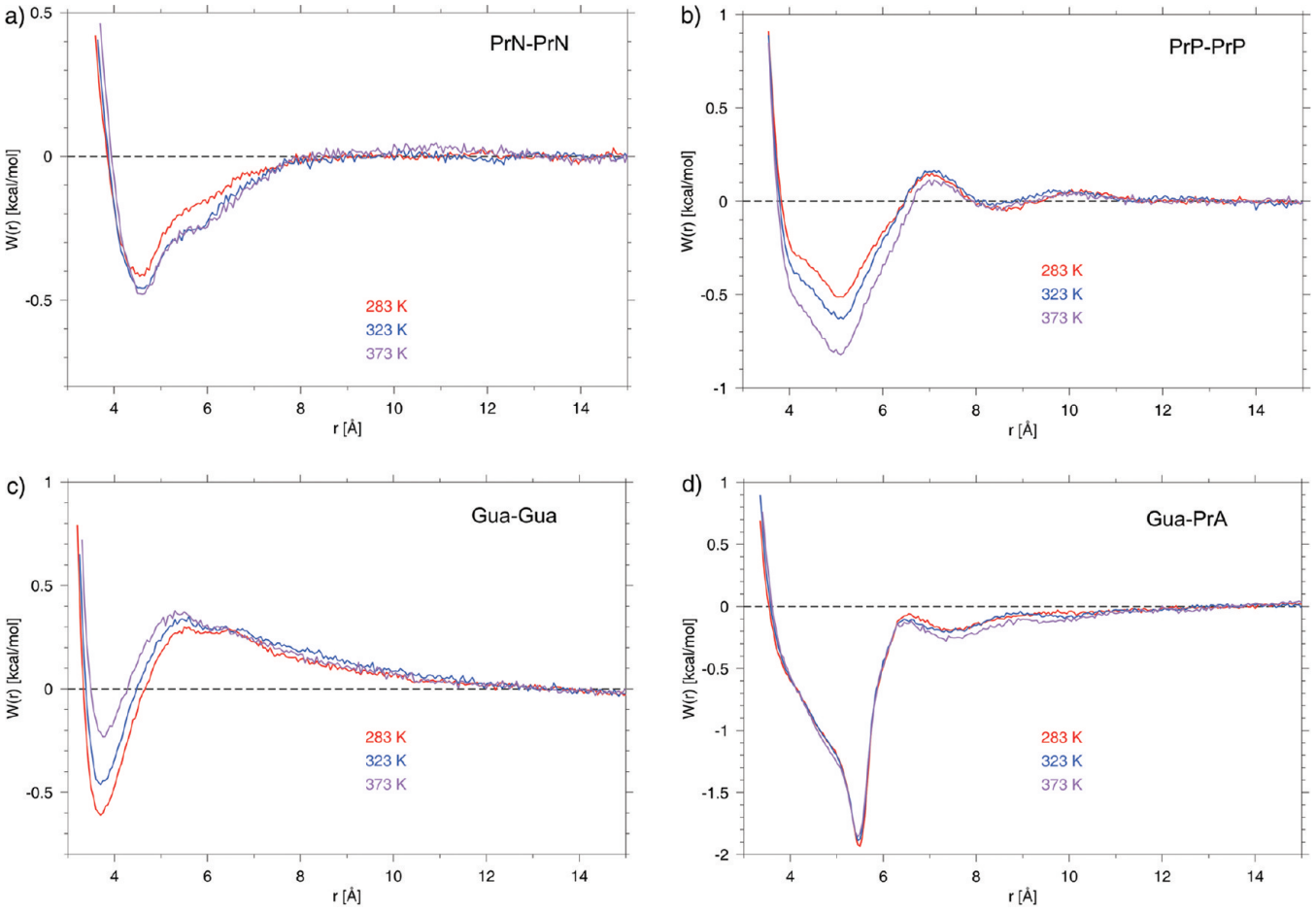

Figure 3. Constant-volume PMF curves for the (a) PrN−PrN, (b) PrP−PrP, (c) Gua−Gua, and (d) Gua−PrA dimers. The red, blue, and purple lines correspond to PMFs determined in the TIP3P water model[14] at temperatures of 283, 323, and 373 K, respectively.

We performed calculations for 15 pairs of molecules to model the interactions between side chains in water. Because of the large number of data, our results can be generally divided into four groups, i.e., (i) systems for which the temperature dependence of the PMFs is not observed; (ii) systems for which the depth of the contact minimum of the PMF increases with temperature; (iii) pairs of positively charged systems; (iv) systems for which PMF does not depend on temperature and the depth of the dimensionless PMF decreases with temperature. In the Results and Discussion section, we present and discuss in detail results for one pair of each mentioned-above group, respectively, PrN−PrN, PrP−PrP, Gua−Gua, and Gua−PrA. The results for the remaining pairs of molecules studied in this work are presented as the Supporting Information.

RESULTS AND DISCUSSION

The PMFs $[W(r;T)$ of eq 2$]$ for the four selected pairs of amino-acid side-chain models PrN−PrN, PrP−PrP, Gua−Gua, and Gua−PrA in water calculated based on MD simulations performed in the NVT scheme at different temperatures are shown in Figure 3a−d. The corresponding dimensionless PMFs $[\tilde{W}(r;T)$ of eq 3$]$ are shown in Figure 4a−d. It can be seen that all PMFs converge to a flat baseline for $r > 11$ Å, which enables us to draw meaningful conclusions as to the quantitative relationships between the PMFs computed at various temperatures.

For the PrN−PrN system (Figure 3a), the depths of the contact minima (the first minimum in the PMF plot at the shortest distances) in the PMF and those of the dimensionless minima vary weakly with temperature. The heights of the desolvation maxima [which occur at larger distances than the contact minima (the first minimum in the PMF plot at the shortest distances) and the depths of the solvent-separated minima (which are next to the contact minima) are almost independent of temperature, or their dependence on temperature is weak. Similar behavior is observed for the EtN−PrN, PrP−EtN, PrA−PrA, PrN−PrA, Gua−PrN, and Gua−PrP (Figures S2a,d,e,h,i,j, respectively, in the Supporting Information).

It can be seen that the depths of the contact minima in the PMF increase with increasing temperature for the PrP−PrP pair (Figure 3b). The same tendency is exhibited by the PrP−PrA, and EtN−PrA pairs, respectively, (Figure S2c,f in the Supporting Information). This means that the entropy of association is positive and is more pronounced than the energy contribution for these systems (because $S = -\partial F/\partial T$, where S denotes entropy, F denotes the free energy, and T denotes absolute temperature, and the PMF can be regarded as restricted free energy). The dimensionless PMFs of the three systems discussed only weakly depend on temperature (compared to regular PMFs), which means that the energy of association is small. This pattern of energy and entropy variation with temperature is characteristic of hydrophobic

dx.doi.org/10.1021/jp212593h | J. Phys. Chem. B 2012, 116, 6844−6853

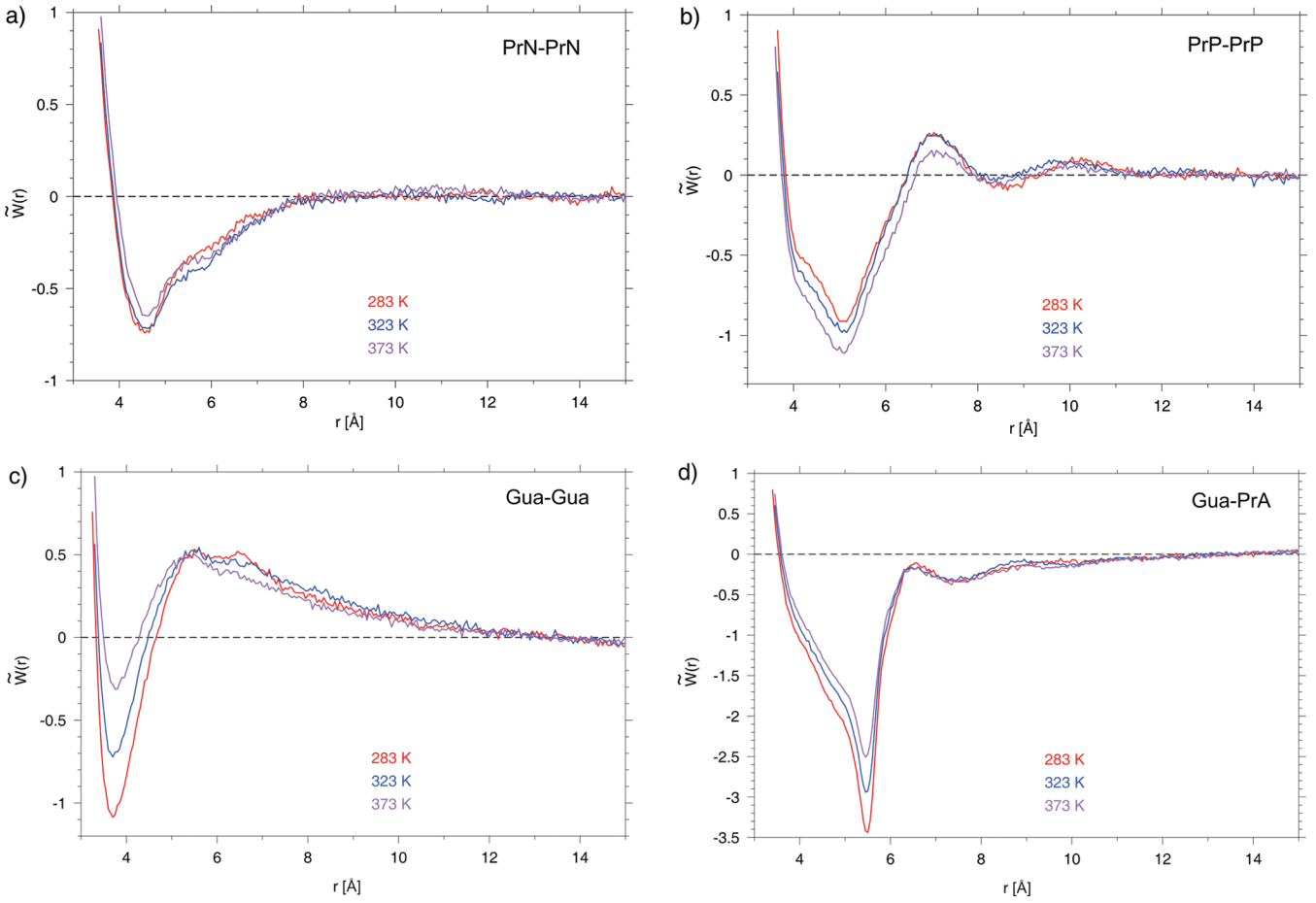

Figure 4. Dimensionless constant-volume PMF curves (each being the negative of the respective pair correlation function) for the (a) PrN−PrN, (b) PrP−PrP; (c) Gua−Gua, (d) Gua−PrA dimers. The red, blue, and purple lines correspond to PMFs determined at temperatures of 283, 323, and 373 K, respectively.

association.[9−12] This result is not surprising for the PrP−PrP and the PrP−PrA pairs but seems to be counterintuitive for the EtN−PrA pair, which can form a salt-bridge. Therefore, for the EtN−PrA pair, the energy of the interaction between the ammonium and carboxylate head groups does not seem to be favorable with respect to the hydration of separated solute particles. It should also be noted that, as opposed to that of the methane dimer in water,[13] the dimensionless PMF of the propane dimer exhibits some weak dependence on temperature (Figure 4b), which is probably caused by the nonspherical shape of propane molecules.

For the Gua−Gua pair (Figure 3c), EtN−EtN (Figure S2g in the Supporting Information), and Gua−EtN (Figure S2k in the Supporting Information) pairs, the depth of the contact minima remarkably decreases (i.e., the PMF increases) with increasing temperature, which means that the entropy increases upon association. This observation can be explained in terms of a stronger electrostatic field created by two fused charged groups compared to two isolated groups, which orders the water molecules more strongly.[32] This observation is supported by the fact that, except for the Gua−EtN system (Figure S3k in the Supporting Information), the depths of the minima in the respective dimensionless PMFs also decrease remarkably (i.e., the dimensionless PMF goes up) with temperature, which demonstrates that energy decreases upon association [because $E = -T^2\partial(F/T)\partial T$]. This energy decrease must be associated with the increase of counterion concentration in the neighborhood of the dimer and, consequently, favorable electrostatic interactions of the solute molecules with them.[24]

It can also be noted that the PMFs of the Gua-PrA pair (Figure 3d), which forms a strong salt-bridge and for the propanamide−propionate anion pair (Figure S2h in the Supporting Information) where strong hydrogen bonds can be formed between the carboxyl oxygen atoms of the propionate anion and the amide hydrogen atoms of propanamide, are virtually independent of temperature, while the depth of the minimum of the dimensionless PMF decreases with increasing temperature (Figure 4d), which suggests that association is energy-driven. Thus, unlike the EtN−PrA pair (Figure S2f of the Supporting Information), the energy of salt-bridge formation in the Gua-PrA pair overcomes that of hydration of isolated solute molecules.

The entropic (thicker lines) and energetic (thinner lines) contribution to the orientation-averaged PMFs are shown as functions of distance in Figure 5a−d for the PrN−PrN, PrP−PrP, Gua−Gua, and Gua−PrA pairs, respectively, and in Figure S4 of the Supporting Information for the remaining systems. On the basis of these plots we observe weak temperature dependence for the PrN−PrN pair (Figure 5a). For this pair, the entropy contribution to the PMF is dominant and has a positive value in the region of the desolvation maximum (at a distance 5−6 Å) and is greater than the energy contribution. The entropy contribution to the PMF is positive in the desolvation-maximum region (at distances close to 5 Å) and

dx.doi.org/10.1021/jp212593h | J. Phys. Chem. B 2012, 116, 6844−6853

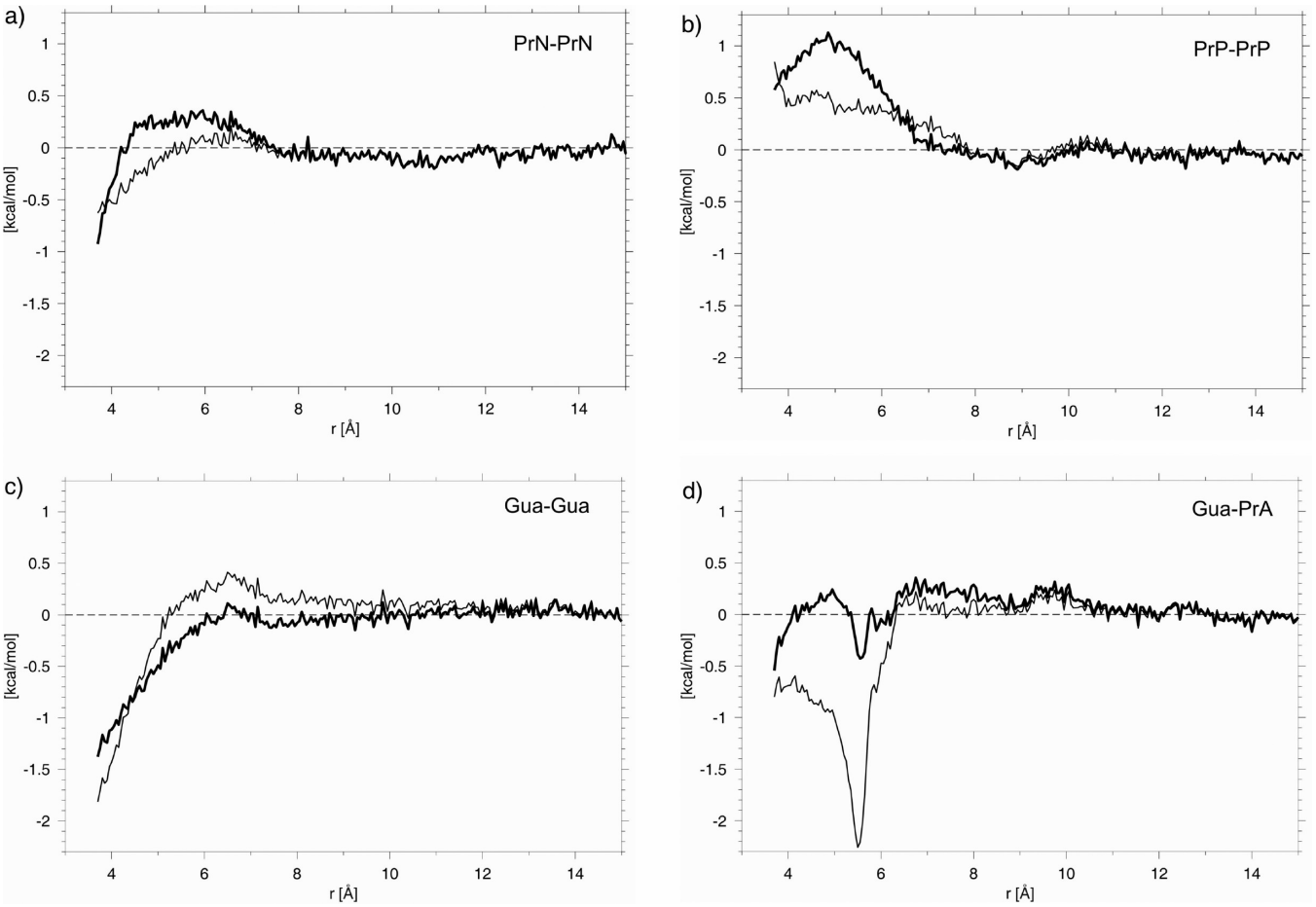

Figure 5. Entropy [expressed as $T\Delta S(r,T)$; thicker lines] and energy [expressed as $\Delta U(r,T)$; thinner lines] contributions to orientation-averaged PMFs for the (a) PrN−PrN, (b) PrP−PrP, (c) Gua−Gua, and (d) Gua−PrA dimers at T = 323 K.

greater than the energy contribution for PrP−PrP (Figure 5b). This behavior is typical of entropy-driven hydrophobic association. As expected from the PMF analysis presented earlier in this section, for the Gua−Gua pair, the energy contribution to the PMF is dominant in the contact-minimum region, while both energy and entropy contributions are negative in the contact-minimum region and positive in the desolvation-maximum region (Figure 5c). The energy contribution for the Gua−PrA (Figure 5d) is negative in the contact-minimum region and is greater than the entropy contribution, thus demonstrating that salt-bridge formation in this system is energy-driven.

Because the side chain-side chain interaction potentials in UNRES depend on distance and orientation,[4] we also analyzed the temperature dependence of the PMFs for three selected orientations, namely, side-to-side (a), head-to-head (b), and head-to-side (c), defined in Figure 6. The PMF and dimensionless PMF curves (plotted as functions of the distance between side-chain centers and orientation) for four pairs of molecules of PrN−PrN, PrP−PrP, Gua−Gua, and Gua−PrA are shown in Figures 7a−d and 8a−d, respectively, as well as Figures S5a−k and S6a−k in the Supporting Information. The solid, dotted, and dashed lines correspond to the PMFs determined for the side-to-side, head-to-head, and head-to-side orientations, respectively. The definitions of those three orientations are indicated on each plot.

The kinds of temperature dependence of the PMFs are summarized in Table 1, where we present the temperature

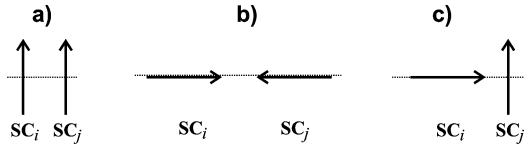

Figure 6. Illustration of the (a) side-to-side, (b) head-to-head, (c) head-to-side orientation of two spheroidal particles. The lines represent the long axes of the spheroids. The orientation variables (see Figure 1 for definition) are (a) $\theta_{ij}^{(1)} = 90°$, $\theta_{ij}^{(2)} = 90°$, and $\phi_{ij} = 0°$; (b) $\theta_{ij}^{(1)} = 0°$, $\theta_{ij}^{(2)} = 180°$, and ϕ_{ij} undefined; and (c) $\theta_{ij}^{(1)} = 0°$, $\theta_{ij}^{(2)} = 90°$, and $\phi_{ij} = 0°$.

dependence of the orientation-averaged and orientation-dependent PMFs and dimensionless PMFs in the region of the contact minima. We defined the temperature dependence as "very weak", "weak" and "strong" if the average change of the depth of the contact minimum from T = 283 K to T = 323 K and from T = 323 K to T = 373 K was 0.05 units or less, 0.05−0.1 units, and more than 0.1 units, respectively, where units are kcal/mol for PMF and natural logarithm units (without physical dimension) for dimensionless PMFs.

It can be seen for side-to-side orientation (solid lines) that each plot possesses a deep contact minimum (occurring at the shortest distances), and a desolvation maximum separating the two minima. Except for the Gua−Gua (Figure 7c), Gua−PrA (Figure 7d), and EtN−EtN (Figure S5g) pairs, the contact minima either shift up in free energy or disappear for the head-to-head and the head-to-side orientations, which results from a

dx.doi.org/10.1021/jp212593h | J. Phys. Chem. B 2012, 116, 6844−6853

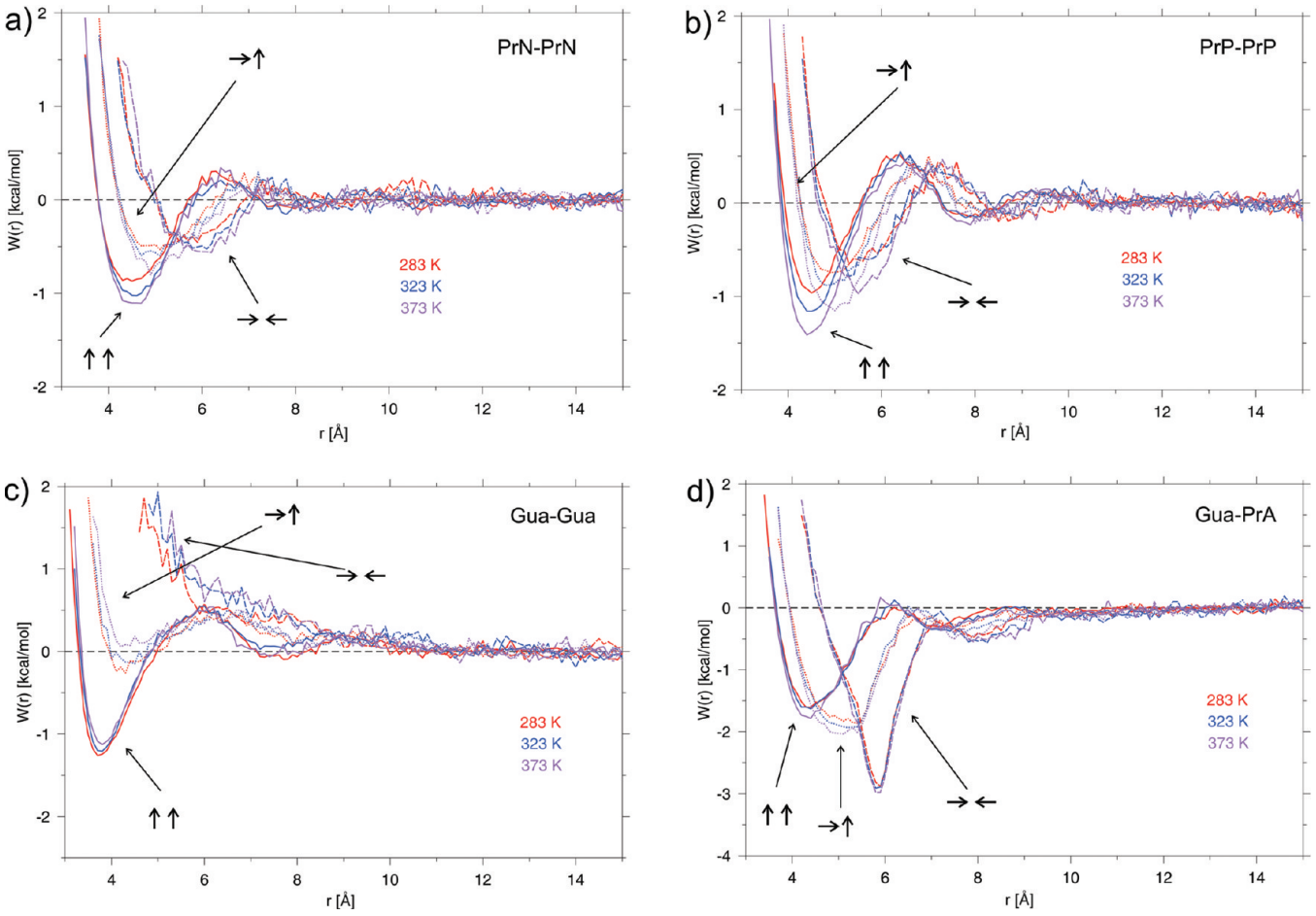

Figure 7. Constant-volume PMF curves for the (a) PrN−PrN, (b) PrP−PrP, (c) Gua−Gua, and (d) Gua−PrA dimers. The solid, dashed, and dotted lines correspond to PMFs determined for the side-to-side (Figure 6a), head-to-head (Figure 6b), and head-to-side (Figure 6c) orientations, respectively. The labels of the respective orientations are shown on the plot. The red, blue, and purple lines correspond to PMFs determined at temperatures of 283, 323, and 373 K, respectively.

close approach of the charged head groups. It should also be noted that the orientation-dependent PMFs of the Gua−Gua pair are similar to that corresponding to a pair of nonpolar PrP−PrP molecules (Figure 7b). On the basis of earlier results of Magalhaes et al.[32] on the analysis of arginine−arginine contact pairs in protein crystal structures, it was observed that such behavior was caused by the presence of the water or counterion bridges between guanidine group. The guanidine group has three nitrogen atoms that can be involved in the formation of water or counterion bridges. In the PMF plot for the Gua−PrA pair, we observe the deepest contact-minimum for the head-to-head orientation (Figure 7d, dashed lines) at all temperatures. The reason for this is that the oppositely charged head groups can make contact with each other for the head-to-head orientations forming a salt bridge, while they are also in contact with the nonpolar parts of the other side chain for the head-to-side and side-to-head orientation.[20] Another reason is that, for these orientations, the electrostatic interactions between the head groups are less attractive because fewer hydrogen bonds can be formed if a carboxylic group faces the side of an ammonium/guanidine group or vice versa. This observation is also supported by the fact that, for pairs that contain the 1-methylguanidinium cation, the minima corresponding to the head-to-head orientation are remarkably deeper compared to those corresponding to the side-to-side orientation. The guanidine group is a large unit and contains five hydrogen-bonding protons which are capable of forming hydrogen bonds when the N−H bonds are nearly colinear with the N···X line, where X denotes proton acceptor. This is consistent with our results[20] for a pair of Arg−Asp (Figure 7d for a pair of Gua−PrA in this work). The curves corresponding to the head-to-head and head-to-side orientations are more ragged than those corresponding to the side-to-side orientations because of poorer statistics. The highest of solvent-separated minima occurred for the negatively charged pair (Figure S5e); they are higher than those for the remaining systems. This observation is in agreement with our earlier results for the distance-dependent PMFs Cl^-−Cl^- pair.[33] The contact minima occur at the shortest distances for the side-to-side (solid lines) and at the longest distances for the head-to-head (dashed lines) orientation. The positions of the desolvation maxima occur at different distances between the centers of the interacting particles, as do those of the contact minima; however, their heights remain constant within the simulation error. It can be seen from Figure 7a−c that, for the side-to-side orientation, the contact minima are wider and deeper for the pairs studied than those for the other orientations. The existence of these minima for this orientation is caused by the fact that more water molecules are eliminated from the side-to-side orientation. The PMF plots dependent on distance and orientation obtained on the basis of MD

dx.doi.org/10.1021/jp212593h | J. Phys. Chem. B 2012, 116, 6844−6853

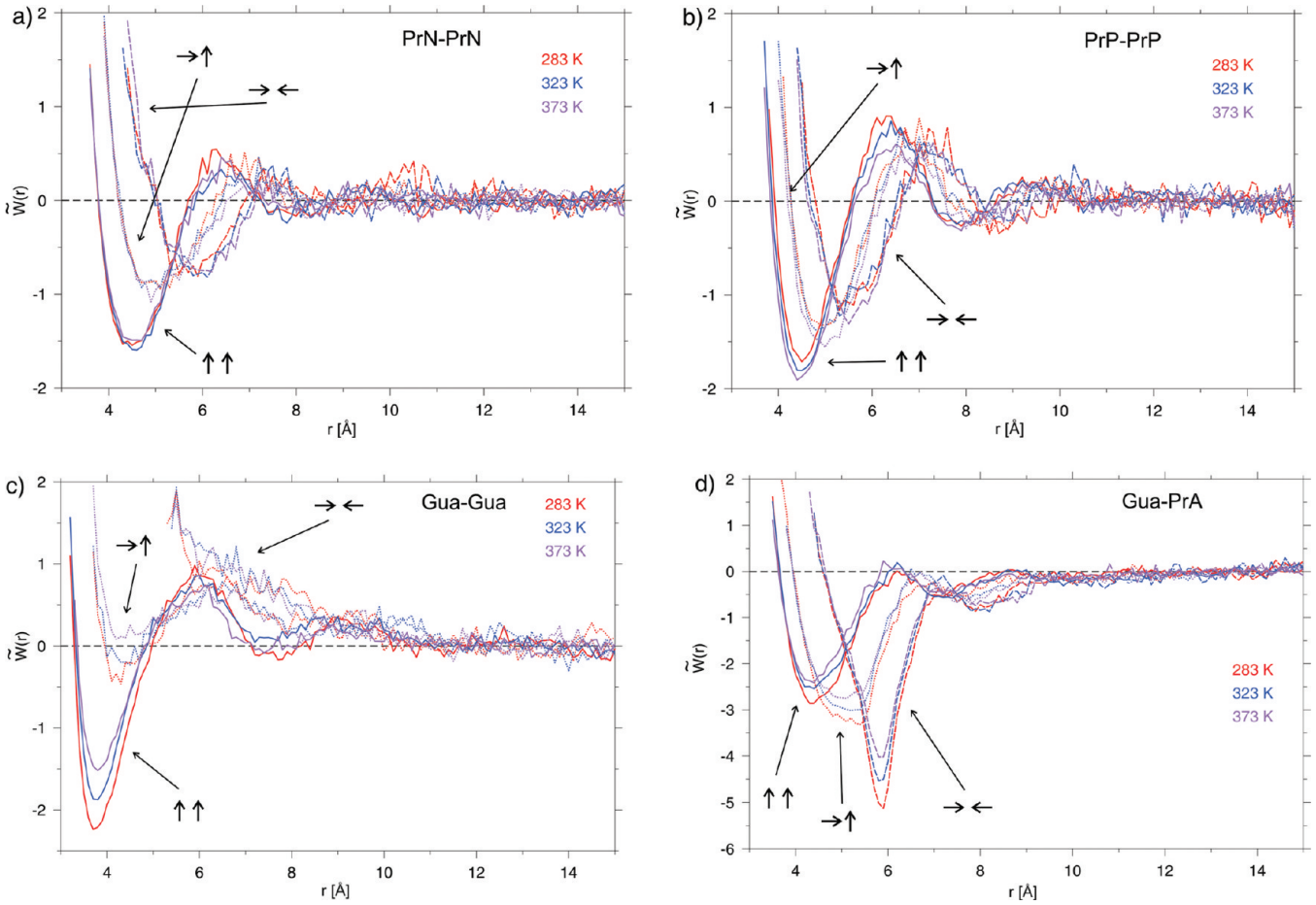

Figure 8. Dimensionless constant-volume PMF curves for the (a) PrN−PrN, (b) PrP−PrP, (c) Gua−Gua, and (d) Gua−PrA dimers. The solid, dashed, and dotted lines correspond to PMFs determined for the side-to-side (Figure 6a), head-to-head (Figure 6b), and head-to-side (Figure 6c) orientations, respectively. The labels of the respective orientations are shown on the plot. The red, blue, and purple lines correspond to PMFs determined at temperatures of 283, 323, and 373 K, respectively.

Table 1. Temperature Dependence in the Region of Contact Minima for the Systems Studied by MD Simulations[a]

	orientation-averaged		orientation-dependent (side−side, side−head, head−head)	
system[b]	PMF	PMF/RT	PMF	PMF/RT
PrN−PrN	W(−)	W(+)	W(−) W(−) W(−)	vW(±) vW(±) vW(±)
PrP−PrP	S(−)	S(−)	S(−) S(−) S(−)	W(−) W(−) W(−)
EtN−PrN	W(−)	W(−)	W(−) W(−) W(−)	W(+) W(+) W(±)
PrP−PrN	vW(−)	S(+)	W(−) W(−) W(−)	S(+) S(+) W(+)
PrP−PrA	S(−)	W(−)	S(−) W(+) W(+)	W(−) W(−) W(−)
PrP−EtN	W(−)	W(−)	W(−) W(−) W(−)	W(−) W(−) W(−)
PrA−PrA	W(+)	W(−)	vW(±) S(+) S(+)	W(−) W(+) S(+)
EtN−PrA	S(−)	W(−)	S(−) S(−) S(−)	vW(−) W(−) vW(−)
EtN−EtN	S(+)	S(+)	W(+) W(+) S(+)	S(+) S(+) S(+)
PrN−PrA	W(−)	W(−)	W(−) W(−) W(−)	W(−) S(±) W(±)
Gua−PrN	W(−)	W(+)	W(−) vW(−) vW(−)	W(+) vW(−) vW(+)
Gua−PrP	W(±)	W(+)	W(±) W(±) W(±)	W(+) W(+) W(+)
Gua−Gua	S(+)	S(+)	W(+) S(+) S(+)	S(+) S(+) W(+)
Gua−EtN	S(+)	W(±)	W(+) S(+) S(+)	W(+) vW(±) vW(±)
Gua−PrA	vW(+)	S(+)	W(−) W(−) vW(−)	S(+) S(+) S(+)

[a]The labels S, W, and vW refer to strong (change greater than 0.1 units), weak (0.05 − 0.1 units), and very weak (0.05 or less units) temperature dependence (where units are kcal/mol for the PMF and natural-logarithm units for dimensionless PMF), respectively. "−" and "+" in parentheses denote the increasing depth of contact minima with increasing temperature, and the decreasing depth of contact minima with increasing temperature, respectively. [b]Abbreviations: PrN − propanamide; PrP − propane; PrA − propionate anion; EtN - ethylammonium cation; Gua − 1-methylguanidinium cation.

dx.doi.org/10.1021/jp212593h | J. Phys. Chem. B 2012, 116, 6844−6853

simulations in water presented in this work are in qualitative agreement with those presented in our earlier papers.[17−20]

It can be noted that, for all three selected orientations (Figure 6), the plots of the PMFs and dimensionless PMFs of the PrP−PrP (Figures 7b and 8b) and the EtN−PrA (Figures S5f and S6f) pairs behave like those of the PMFs averaged over all orientations. However, the PMF of the PrP−PrA pair (Figures S5c) exhibits strong temperature dependence only for the side-to-side orientation, at which the nonpolar faces make the most efficient contacts, while there is only weak temperature dependence for the side-to-head and head-to-head orientations at which the polar headgroup of PrA contacts PrP. The temperature dependence characteristic of the respective orientation-averaged PMFs and dimensionless PMFs is also preserved in distance- and orientation-dependent PMFs and dimensionless PMFs of the PrP−PrN (Figures S5b and S6b) and the Gua−PrA (Figures 7d and 8d) systems. For the three positively charged-pair systems (Gua−Gua, EtN−EtN, and Gua−EtN), the depths of the minima in the PMF weakly depend on temperature for the side-to-side orientation, while they strongly decrease with increasing temperature for the side-to-head and head-to-head orientations (Figures 7c, S5g, and S5k, respectively). Conversely, the depths of the minima in the dimensionless PMFs strongly decrease with temperature for the side-to-side orientation, while the temperature dependence is weak for the side-to-head and head-to-head orientation (Figures 8c, S6g, and S6k, respectively). Therefore, the association seems to be driven by energy when the nonpolar tails and polar head groups approach each other simultaneously for the side-to-side orientation and seems to be driven by entropy for the other orientations.

CONCLUSIONS

The results of the study reported in this work as well as those of our previous work[13] strongly suggest that the dimensionless PMFs of pairs of nonpolar solutes depend more weakly on temperature in the region of contact minimum than the PMF. This is consistent with the fact that hydrophobic association is an entropy-driven phenomenon. The PMF does not vary remarkably with temperature in the region of the desolvation maximum and of the solvent-separated minimum. Additionally, in this study, we found that the potentially salt-bridge-forming EtN−PrA pair follows the same temperature-dependence pattern. On the other extreme are the Gua−PrA and PrP−PrN pairs, for which the PMF is virtually independent of temperature, and the depth of the contact minimum of the dimensionless PMF decreases with temperature, which means that association is driven by energy. The reason for this is probably the branched head groups of both solute molecules, one of which is a donor and the other one is an acceptor in hydrogen bonding; consequently, the energy of hydrogen-bond formation overcomes that of solvation of isolated solute molecules.

For the PrP−PrA pair, the association process seems to be driven by entropy (strong decrease of the PMF with temperature, but not of the dimensionless PMF, with increasing temperature for the side-to-side orientation); however, this observation does not translate to the PrP−EtN pair for which the PMF and the dimensionless PMF weakly depend on temperature. Finally, for the pairs composed of positively charged solute molecules, the side-to-side association seems to be entropy-driven, and the side-to-head and head-to-head association seem to be energy-driven. Again, this observation does not translate to the PrA−PrA pair (in which both solute molecules are negatively charged), the PMF and dimensionless PMF of which weakly depend on temperature. The PMFs and the dimensionless PMFs of the remaining pairs, most of which consist of polar or polar and nonpolar residues, exhibit no remarkable temperature dependence. It should also be noted that the temperature dependence of the PMF does not seem to be separable to contributions coming from the interactions of nonpolar and charged groups.

From the results of this study, we can conclude that, as far as coarse-grained force fields are concerned, there is a need to introduce temperature dependence of the potentials of interaction of (a) pairs of nonpolar side chains, (b) Lys−Asp and Lys−Glu pairs, (c) pairs of positively charged side chains, and (d) pairs composed of negatively charged and nonpolar side chains. As proposed in our earlier work,[13] the temperature-dependent potentials of categories (a) and (b) could be derived by scaling the reference potentials by temperature or, more rigorously, by combining the observations that the depth of the minimum of the dimensionless PMF dependent on distance and orientation $[\tilde{W}(r,\theta^{(1)},\theta^{(2)},\phi;T)]$ and the height of the desolvation maximum of the PMF $[W(r,\theta^{(1)},\theta^{(2)},\phi;T)]$ are independent of temperature. Then PMF fitting could be carried out under the conditions given by eqs 9 and 10.

$$\frac{\partial \tilde{W}(r,\theta^{(1)},\theta^{(2)},\phi,T)}{\partial T} \equiv 0 \quad \text{at the contact minimum} \tag{9}$$

$$\frac{\partial W(r,\theta^{(1)},\theta^{(2)},\varphi,T)}{\partial T} \equiv 0 \quad \text{at the desolvation maximum} \tag{10}$$

The potentials of categories (c) and (d) require more consideration because the dependence on temperature is coupled with the dependence on orientation. Work on this problem and implementation of the potentials in the UNRES force field is currently being carried out in our laboratory.

ASSOCIATED CONTENT

Supporting Information

Table S1: box dimensions and number of water molecules for the systems studied by MD simulations. Figure S1: partial atomic charges (in electron charge units) of propanamide, propane, propionate anion, ethylammonium cation, and 1-methylguanidinum cation molecules calculated by using the RESP method[29] based on HF/6-31G* calculations carried out with GAMESS[28] used in the calculations with the AMBER force field. Figure S2: constant-volume PMF curves for the EtN−PrN, PrP−PrN, PrP−PrA, PrP−EtN, PrA−PrA, EtN−PrA, EtN−EtN, PrN−PrA, Gua−PrN, Gua−PrP, and Gua−EtN dimers determined at temperatures of 283, 323, and 373 K, respectively. Figure S3: dimensionless constant-volume PMF curves for the EtN−PrN, PrP−PrN, PrP−PrA, PrP−EtN, PrA−PrA, EtN−PrA, EtN−EtN, PrN−PrA, Gua−PrN, Gua−PrP, and Gua−EtN dimers determined at temperatures of 283, 323, and 373 K, respectively. Figure S4: entropy and energy contributions to absolute PMFs for the EtN−PrN, PrP−PrN, PrP−PrA, PrP−EtN, PrA−PrA, EtN−PrA, EtN−EtN, PrN−PrA, Gua−PrN, Gua−PrP, and Gua−EtN dimers plotted at T = 323 K. Figure S5: constant-volume PMF curves for the EtN−PrN, PrP−PrN, PrP−PrA, PrP−EtN, PrA−PrA, EtN−PrA, EtN−EtN, PrN−PrA, Gua−PrN, Gua−PrP, and Gua−EtN dimers determined at temperatures of 283, 323, and 373 K,

dx.doi.org/10.1021/jp212593h | J. Phys. Chem. B 2012, 116, 6844−6853

respectively. Figure S6: dimensionless constant-volume PMF curves for the EtN−PrN, PrP−PrN, PrP−PrA, PrP−EtN, PrA−PrA, EtN−PrA, EtN−EtN, PrN−PrA, Gua−PrN, Gua−PrP, and Gua−EtN dimers determined at temperatures of 283, 323, and 373 K, respectively. This material is available free of charge via the Internet at http://pubs.acs.org.

AUTHOR INFORMATION

Corresponding Author

*E-mail: momo@chem.univ.gda.pl.

Notes

The authors declare no competing financial interest.

ACKNOWLEDGMENTS

This research was conducted by using the resources of (a) our 818-processor Beowulf cluster at the Baker Laboratory of Chemistry and Chemical Biology, Cornell University, (b) the National Science Foundation Terascale Computing System at the Pittsburgh Supercomputer Center, (c) our 45-processor Beowulf cluster at the Faculty of Chemistry, University of Gdańsk, (d) the Informatics Center of the Metropolitan Academic Network (IC MAN) in Gdańsk, and (e) the Interdisciplinary Center of Mathematical and Computer Modeling (ICM) at the University of Warsaw. This work was supported by grants from the U.S. National Institutes of Health (GM-14312), the U.S. National Science Foundation (MCB05-41633), and the Polish Ministry of Science and Education (N N204 152836).

REFERENCES

(1) Seetharamulu, P.; Crippen, G. M. *J. Math. Chem.* **1991**, *6*, 91−110.
(2) Koliński, A.; Skolnick, J. *Proteins* **1994**, *18*, 338−352.
(3) Koliński, A.; Skolnick, J. *Proteins* **1994**, *18*, 353−366.
(4) Liwo, A.; Ołdziej, S.; Pincus, M. R.; Wawak, R. J.; Rackovsky, S.; Scheraga, H. A. *J. Comput. Chem.* **1997**, *18*, 849−873.
(5) Liwo, A.; Khalili, M.; Czaplewski, C.; Kalinowski, S.; Ołdziej, S.; Wachucik, K.; Scheraga, H. A. *J. Phys. Chem. B* **2007**, *111*, 260−285.
(6) Liwo, A.; Pillardy, J.; Czaplewski, C.; Scheraga, H. A. *J. Chem. Phys.* **2001**, *115*, 2323−2347.
(7) Némethy, G.; Scheraga, H. A. *J. Phys. Chem.* **1962**, *66*, 1773−1789.
(8) Dill, K. A. *Biochemistry* **1990**, *29*, 7133−7155.
(9) Lüdemann, S.; Schreiber, H.; Abseher, R.; Steinhauser, O. *J. Chem. Phys.* **1996**, *104*, 286−295.
(10) Shimizu, S.; Chan, H. S. *J. Chem. Phys.* **2000**, *113*, 4683−4700.
(11) Paschek, D. *J. Chem. Phys.* **2004**, *120*, 6674−6690.
(12) Paschek, D. *J. Chem. Phys.* **2004**, *120*, 10605−10617.
(13) Sobolewski, E.; Makowski, M.; Ołdziej, S.; Czaplewski, C.; Liwo, A.; Scheraga, H. A. *Protein Eng., Des. Sel.* **2009**, *22*, 547−552.
(14) Jorgensen, W. L.; Chandrasekhar, J.; Madura, J. D.; Impey, R. W.; Klein, M. L. *J. Chem. Phys.* **1983**, *79*, 926−935.
(15) Makowski, M.; Liwo, A.; Scheraga, H. A. *J. Phys. Chem. B* **2007**, *111*, 2910−2916; **2010**, *114*, 1226 (Erratum).
(16) Makowski, M.; Liwo, A.; Maksimiak, K.; Makowska, J.; Scheraga, H. A. *J. Phys. Chem. B* **2007**, *111*, 2917−2924.
(17) Makowski, M.; Sobolewski, E.; Czaplewski, C.; Liwo, A.; Ołdziej, S.; No, J. H.; Scheraga, H. A. *J. Phys. Chem. B* **2007**, *111*, 2925−2931.
(18) Makowski, M.; Sobolewski, E.; Czaplewski, C.; Ołdziej, S.; Liwo, A.; Scheraga, H. A. *J. Phys. Chem. B* **2008**, *112*, 11385−11395.
(19) Makowski, M.; Liwo, A.; Sobolewski, E.; Scheraga, H. A. *J. Phys. Chem. B* **2011**, *115*, 6119−6129.
(20) Makowski, M.; Liwo, A.; Scheraga, H. A. *J. Phys. Chem. B* **2011**, *115*, 6130−6137.
(21) Czaplewski, C.; Rodziewicz-Motowidło, S.; Liwo, A.; Ripoll, D. R.; Wawak, R. J.; Scheraga, H. A. *Protein Sci.* **2000**, *9*, 1235−1245.
(22) Czaplewski, C.; Ripoll, D. R.; Liwo, A.; Rodziewicz-Motowidło, S.; Wawak, R. J.; Scheraga, H. A. *Int. J. Quantum Chem.* **2002**, *88*, 41−55.
(23) Czaplewski, C.; Rodziewicz-Motowidło, S.; Dąbal, M.; Liwo, A.; Ripoll, D. R.; Scheraga, H. A. *Biophys. Chem.* **2003**, *105*, 339−359.
(24) Czaplewski, C.; Kalinowski, S.; Liwo, A.; Ripoll, D. R.; Scheraga, H. A. *Mol. Phys.* **2005**, *103*, 3153−3167.
(25) Pearlman, D. A.; Case, D. A.; Caldwell, J. W.; Ross, W. S.; Cheatham, T. E., III; DeBolt, S.; Ferguson, D.; Seibel, G.; Kollman, P. A. *Comput. Phys. Commun.* **1995**, *91*, 1−41.
(26) Case, D. A.; Pearlman, D. A.; Caldwell, J. W.; Chaetham, T. E., III; Wang, J.; Ross, W. S.; Simmerling, C. L.; Darden, T. A.; Merz, K. M.; Stanton, R. V.; et al. *AMBER 7*; University of California: San Francisco, CA, 2002.
(27) Miyamoto, S.; Kollman, P. A. *J. Comput. Chem.* **1992**, *13*, 952−962.
(28) Schmidt, M. W.; Baldridge, K. K.; Boatz, J. A.; Elbert, S. T.; Gordon, M. S.; Jensen, J. A.; Koseki, S.; Matsunaga, N.; Nguyen, K. A.; Su, S.; et al. *J. Comput. Chem.* **1993**, *14*, 1347−1363.
(29) Bayly, C. I.; Cieplak, P.; Cornell, W. D.; Kollman, P. A. *J. Phys. Chem.* **1993**, *97*, 10269−10280.
(30) Kumar, S.; Bouzida, D.; Swendsen, R. H.; Kollman, P. A.; Rosenberg, J. M. *J. Comput. Chem.* **1992**, *13*, 1011−1021.
(31) Kumar, S.; Rosenberg, J. M.; Bouzida, D.; Swendsen, R. H.; Kollman, P. A. *J. Comput. Chem.* **1995**, *16*, 1339−1350.
(32) Magalhaes, A.; Maigret, B.; Hoflack, J.; Gomes, J. N.; Scheraga., H. A. *J. Protein Chem.* **1994**, *13*, 195−215.
(33) Maksimiak, K.; Rodziewicz-Motowidło, S.; Czaplewski, C.; Liwo, A.; Scheraga, H. A. *J. Phys. Chem. B* **2003**, *107*, 13496−13504.